Dynamics of Momentary Reserves in Different Grid Topologies under Contingency: Observations from Numerical Experiments

Kosisochukwu Pal Nnoli
Dept. of Computer Science and Electrical Engineering
Jacobs University, 28759 Bremen
Bremen, Germany
email: k.nnoli@jacobs-university.de

Stefan Kettemann
Dept. of Physics and Earth Science and Dept. of Computer Science
Jacobs University, 28759 Bremen
Bremen, Germany
Division of Advanced Materials Science, Pohang 790-784
South Korea
email: s.kettemann@jacobs-university.de

***Abstract*—This paper presents the studies and investigations on the dynamics and mechanism of momentary reserves contribution in electrical power systems under contingency. Momentary reserve through the machine's inertia serves the purpose of primary frequency control and prevents voltage collapse in the case of reactive power reserves. A simulation was performed on a realistic Nigerian 330 kV transmission network in PowerFactory software to study and investigate the mechanism of these reserve functions on the network buses as an inertia active power control method. Moreover, we investigated the influence of geodesic increment of momentary reserve on the decay of disturbances and in turn estimated the value of the post contingent frequency at the network buses. The results indicated that the momentary reserve by inertia alone reduces the frequency deviation from its nominal value, delays the transmission of disturbances and enhances the damping of oscillations by reducing the final frequency settling time at the buses under contingency. These results were further extrapolated by the numerical experiments carried out on a synthetic Square 330 kV power network to account for the effects of meshedness as a distinguishing factor in grid topologies. These numerical experiments also suggest the optimal placement of the momentary reserves in the grid in order to improve system stability against power outage disturbances.**

***Index Terms*—momentary reserves; system perturbation; inertia control, oscillations damping; grid meshedness.**

I. Introduction

The active and reactive power reserves of synchronous generators or Battery Energy Storage Systems (BESS) are the keys to a successful system control in power systems. For each power generator in the grid, power reserve represents the total amount of power remaining after the supply of system loads and losses. The definition and importance of many power reserves have been discussed in [1] and would be reiterated here. This definition of power reserves does not extend to exceeding the power capability curve of the generators. These reserves are particularly referred to as spinning reserves in synchronous machines more than in other kinds of power generators, like the wind and solar generators using BESS [2]. These power reserves can be used for both or either primary frequency control, secondary control and tertiary control [3] [4] [5]. Again, not all of these remaining power reserves from generators are assigned for primary control function alone, we classify the ones momentarily made available through the generators' droop functions specifically for few seconds primary frequency and active power control as momentary reserves of the generators. A lot about system stability and reliability rest on the grid's momentary reserves.

The control and response of generators to network disturbances or contingencies depend heavily on the kind and magnitude of the disturbance and amount of momentary reserves available for use in the primary frequency control or in voltage security. Since primary control requires fast control action to be taken within few seconds of contingency, momentary reserves and their placement play important roles in the dynamics of the disturbance from the point of contingency (PoC) or fault location to the rest of the electrical power network. In this paper, we investigate how the dynamics of a disturbance is influenced by momentary reserves first at the contingent node, its neighbour nodes and other nodes located far away from the fault location. We would see whether a disturbance is damped as it travels across a grid and whether it could be contained on fewer nodes (i.e., localized) based on the function of the grid's momentary reserves. These investigations are carried out in the DigSILENT PowerFactory software [6], using the Nigerian 330 kV grid as a case study. In order to account for a distinctive grid topology characteristic, we would also consider a synthetic Square 330 kV power network as another case study because of its high degree of meshedness.

In this paper, we would start with a brief literature review of reserve functions in Section II. We would then proceed with the description, modeling and simulation of our test transmission networks in Section III. In Section IV, we would investigate the dynamics of momentary reserve on the test networks with a concise summary of the results in Section V and conclude with our findings and recommendation in Section VI.

II. Literature Review

For many years, synchronous machine reserves have been the major source of power compensation in complex power grids prior to the popularity and grid integration of major successful storage devices like the BESS and hydrogen storage. These power compensation reserves, now from both synchronous machines and other storage sources can be called on during grid contingencies, especially in power outage events due to loss of generators or major transmission lines to ensure sufficient system frequency oscillation damping, control and stability. These power reserves can be categorized as momentary, primary, secondary and tertiary based on the grids' request time, duration and magnitude of need of them as shown in Figure 1.

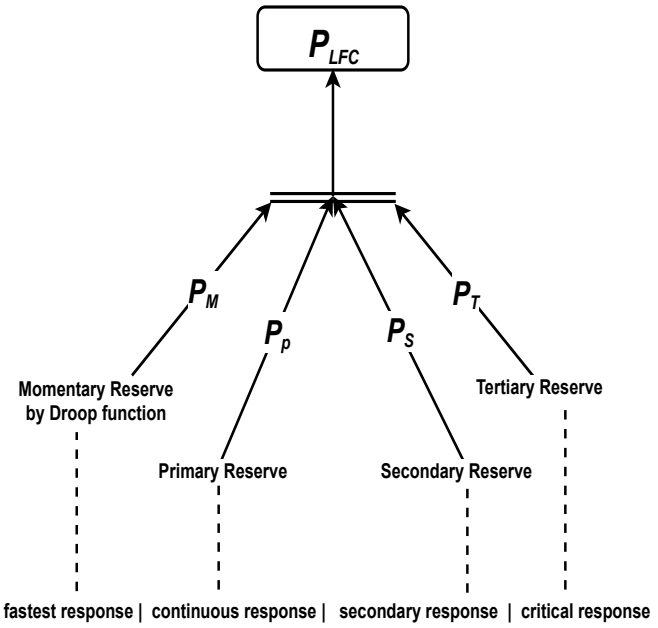

Figure 1: Categorization of Power Reserves based on Grid's Compensation needs in request time, duration and magnitude. P_{LFC} indicates power reserves injected at low frequency contingencies.

According to [3] [4] [7], the time, duration and magnitude factors characterizing the need for grid's power compensation are determined by forecast and sudden imbalances between the power generation, consumption, losses and minutes to hourly contingencies. While the primary reserves are expected to be fully activated within 30 seconds of local request time, the secondary reserves are expected to be automatically and fully activated between 10 to 15 minutes of request time in order to restore power balance and to bring the frequency back to its nominal value. The tertiary reserves account for additional dispatches possible through market negotiations to bring the grid to stability in case of prolonged contingencies, which could not be handled by finite continuous response of secondary reserves. While the secondary and tertiary reserves are controlled and implemented by system operators and where multiple network authorities may be involved [7] [8], the momentary reserves, which are constantly available by droop call function within seconds (i.e., fastest response) followed by continuous response (i.e., primary reserves) made available through agreements between the grid operators and power generating firms for quarterly compensation or contingency purposes are our focus in this numerical experiments. Many authors have carried out extensive research on the effects and importance of primary, secondary and tertiary control reserves [9]–[11]. Machowski, Bialek and Bumby in [4] have confirmed the importance of primary frequency control to the overall frequency stability of the network, especially for inter-area modes of oscillation. A new nonlinear droop control function was studied for wind turbine in [12] where a new dynamic droop coefficient is connected as the negative feedback of the original droop control coefficient in order to bring the product of the original droop control coefficient and nominal frequency within a controllable range. This was done in real time according to the target frequency to improve the primary frequency control. The adaptive droop control action was simulated to show its frequency control rate but there was no concrete understanding of the mechanism of this action on the network bus rather than reducing the frequency dip at post-contingency. This means that little has been numerically investigated to practically understand the mechanics and mechanisms of contribution of momentary control reserves in the stability of power grids. We predict that these first few seconds of primary control response determines the system's need for continuous (i.e., full activation of primary control reserves) and secondary reserves and is therefore essential to system recovery from contingencies. As a result, this paper is directed towards studying the numerical mechanics of dynamics and effective distribution of control response function of momentary reserves at a fault event in realistic model of Nigerian network and a Square grid in order to account for varying network topologies.

III. Modeling and Simulation of the Nigerian Transmission Network Model

To understand our case study system and its parameter interactions, we would describe the components that make up the network. The Nigerian 330 kV transmission grid consist of $N_S = 71$ substations/nodes, $N_L = 81$ over-head transmission lines (made from an alloy of aluminium and steel) with an average length of 92 km, each with a limiting current of 1320 A. The grid is comprised of 107 less-decommissioned units of generators, accounting for the present 29 power stations. The apparent power capacity of the Nigerian grid is about $13,208MW$ as of 2020 [13]. There are other lower voltage networks including the 132 kV and 33 kV sub-transmission networks. For household utilities, there are 11 kV and 0.415 kV 3-phase distribution networks. The Nigerian network operates at $\nu_0 = 50$ Hz frequency and can be described as a grid where most of the nodes are connected to one another in a ring form [14], as seen in the diagram shown in Figure 2.

To control the voltage outputs of the generators through their excitation control, the simplified excitation Automatic Voltage Regulator (AVR) model is used [15]. Other controllers

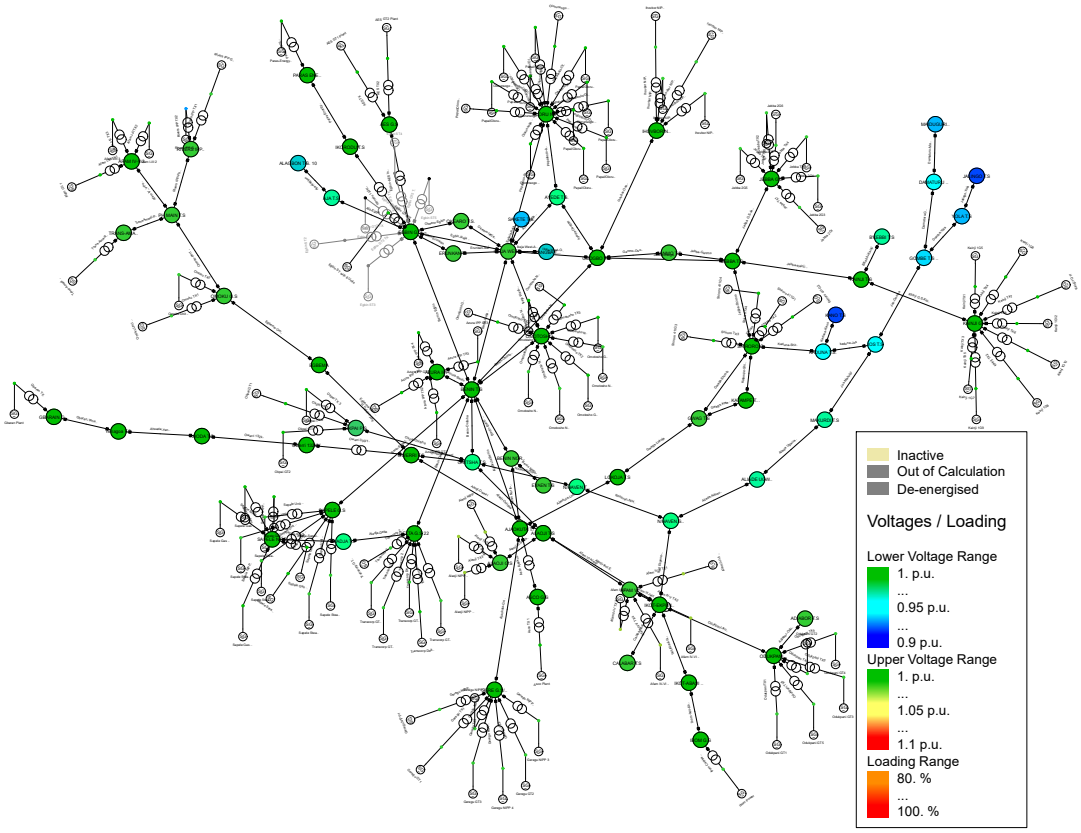

Figure 2: The Nigerian 330 kV Electrical Power Grid.

include power system stabilizers (PSS2A-model) tasked with enhancing the damping of the entire power system's oscillations through excitation control.

The input signal to the PSS2A controller is the derivative of generator's rotor speed and its output is injected to the AVR through the excitation system. This injection works to terminate the phase-lag between the voltage reference and the windings' torque of the generator [16]. For the synchronous machine model, the choice of the model is influenced by the IEEE guide in [17]. The speed governor in the model is the Turbine Governor (TGOV) model used to maintain the frequency operational limits according to swing equation [18]. Here, the swing equation describes the torque balance between the mechanical torque T_t in N.m. of each synchronous machine's turbine and the electromagnetic torque T_e in N.m. as governed by the differential equation given as [3] [4] [11],

$$J_i \frac{d\omega_i^{\Theta}}{dt} + D_{r_i}\omega_i^{\Theta} = T_t - T_e - D_{r_i}\omega_0, \tag{1}$$

where $J_i = \frac{2H_i}{\omega_0^2} S_i$ is the combined moment of inertia of the generator and turbine in kg.m^2 with H_i the generator inertia constant in seconds and S_i the generator apparent power in Volt-Amperes (VA). D_{r_i} represents the rotational loss due to generator rotor windings for each i^{th} generator in N.m.s and i denotes the index of power generators in the grid. Here, t is time in seconds and ω_i^{Θ} is the angular velocity of the rotor in electrical rad/s with ω_0 as its rated synchronous value in electrical rad/s. If we assume that a change in the rotor's angular velocity $(\omega_i^{\Theta} - \omega_0)$ is a derivative of its angular position δ in electrical radians with respect to its rotating setpoint, δ_0 at t $= 0$ given as

$$\omega_i^{\Theta} - \omega_0 = \frac{d\delta_i}{dt}, \tag{2}$$

then, with respect to time, the derivative of ω_i^{Θ} would give

$$\frac{d\omega_i^{\Theta}}{dt} = \frac{d}{dt}\left(\frac{d\delta_i}{dt}\right) + \frac{d\omega_0}{dt}, \tag{3}$$

where ω_0 is the constant rated synchronous value whose derivative with respect to time gives zero (i.e., $\frac{d\omega_0}{dt} = 0$), (3) becomes,

$$\frac{d\omega_i^{\Theta}}{dt} = \frac{d^2\delta_i}{dt^2}. \tag{4}$$

In practice, ω_0 is related to the grid frequency (v_o) by $2\pi v_o$, where v_o is 50 Hz in the Nigerian power grid. If we represent the net mechanical shaft torque at grid frequency to be $T_m = T_t - D_{r_i}\omega_0$, substituting (4) into (1), we then have,

$$J_i \frac{d^2\delta_i}{dt^2} + D_{r_i}\left(\frac{d\delta_i}{dt}\right) = T_m - T_e. \tag{5}$$

Here, we assumed that the network perturbation effected on the rotors from the fault location is small. Multiplying both

sides of (5) by the rated speed (ω_0) in order to ensure that we maintain a synchronous 50 Hz revolution throughout the system, balancing the power, we have

$$J_i\omega_0\frac{d^2\delta_i}{dt^2}+D_{r_i}\omega_0\left(\frac{d\delta_i}{dt}\right)=T_m\omega_0-T_e\omega_0. \quad (6)$$

As power $P=T\omega$, the right side of (6) can now be written as

$$J_i\omega_0\frac{d^2\delta_i}{dt^2}+D_{r_i}\omega_0\left(\frac{d\delta_i}{dt}\right)=P_m-P_e, \quad (7)$$

where P_m is the turbine's mechanical power and P_e is the generator's air-gap electrical power. If we represent the rotor angular momentum at rated speed with M_i (i.e., $M_i=J_i\omega_0=\frac{2H_i}{\omega_0}S_i$) and also represent the damping coefficient at rated synchronous speed with D_i (i.e., $D_i=D_{r_i}\omega_0$), the swing equation can then be re-written in many forms as,

$$M_i\frac{d^2\delta_i}{dt^2}+D_i\frac{d\delta_i}{dt}=P_{m,i}-P_{e,i}, \quad (8)$$

and also as [19] [20],

$$\frac{2H_i}{\omega_o}S_i\frac{d^2\delta_i}{dt^2}+D_i\frac{d\delta_i}{dt}=P_i+\sum_{j=1}^{N_S}W_{ij}\sin(\delta_j-\delta_i), \quad (9)$$

where P_i is the power in the grid's i^{th} node, N_S is the number of nodes/buses and $W_{ij}=V_iV_jB_{ij}$ is the power capacity in Watt of the transmission lines and it is dependent on the network voltage with $\sin(\delta_j-\delta_i)$ modeling the dependence of their phase differences, which informs the direction of powerflow and the transmission of disturbances in the case of contingencies. We performed load-flow calculations using the Newton-Raphson method and electromechanical simulations in DigSILENT PowerFactory software, as documented in [21]. Here, we report results applying these simulations to study the effect of momentary reserves on system dynamics and its contribution to the overall system stability.

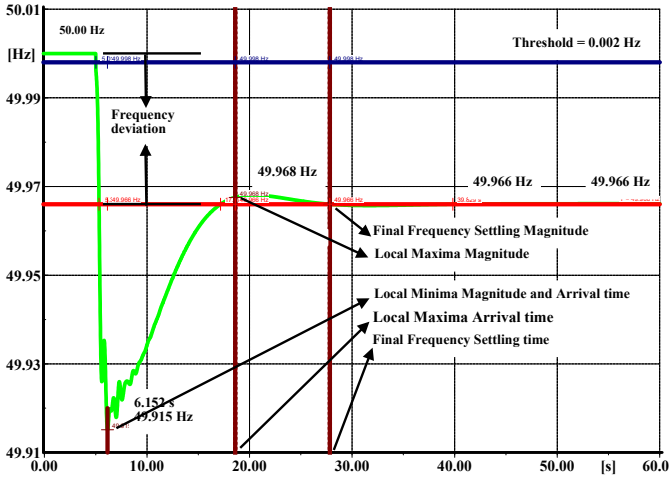

Figure 3: Green Line: Frequency as a function of time at a node where a Synchronous Machine (SM) event occurred at $t=5$s.

IV. Dynamics of Momentary Reserve

For a power system to be in a balanced state, the total power generated (P) has to be equal to the sum of the total load and the transmission losses (P^{x}). This means that for the system to always remain balanced, any change in the load demand and/ losses would require a balancing change in the generated power P. Therefore, the condition $\Delta P >> \Delta P^{\mathrm{x}}$ should always be fulfilled to ensure the security and integrity of power grids. These dynamic changes result in a permanently changing frequency according to the speed-droop characteristics of power turbines, given by [4]

$$\frac{\Delta\nu_i}{\nu_0}=-\sigma_i\frac{\Delta P_i}{P_i^{\mathrm{x}}}, \quad (10)$$

where ν_0 is the nominal frequency in Hertz and σ_i is the local droop of the generation characteristics at the i^{th} generator node, $\sigma_i=P_i^{\mathrm{x}}/P_i$. Thus, any change in frequency resulting from a change in load demand or losses requests a generator response. In this way, if the node is a synchronous generator node, its inertia is expected to slow down the transmission of disturbances to other nodes connected to it, while attempting to damp the frequency oscillations with its momentary reserve according to its droop σ_i function. However, its ability to do so depends on the amount of momentary reserve that the generator can supply, according to its dead zone speed-droop characteristics setting (i.e., possibility of ΔP_i and in the absence of no generator overload in the case of sudden load injection). Since it is not feasible to inject power equally at every node, we aim to understand the dynamics of these reserves to see how an available momentary reserve at one node influences the frequency dynamics at other nodes as function of their distance from the fault location. A better understanding of this influence in the realistic Nigerian grid model would be advantageous for its optimal placement and could improve primary frequency control in real power grids.

To show the influence of geographical distribution of inertia with available momentary reserve, we chose the Nigerian transmission grid as the case study grid. As reported in Section III, we modelled this network in PowerFactory software and calculated the load flow of the network. We considered the voltage dependency of grid loads, and the active power control according to the grid inertia. The effect of provision of momentary reserves by system inertia on the frequency stability of the electrical power networks is studied by varying the aggregated inertia constant H_{agg} of the entire grid, as defined by [22] [23],

$$H_{\mathrm{agg}}=\frac{\sum_{i=1}^{N_S}H_iS_i}{S_n}, \quad (11)$$

where S_i and H_i are the rated apparent power and inertia constant of the i^{th} bus, respectively, $S_n=\sum_{i=1}^{N_S}S_i$ is the total rated power in the grid. Note that H_i on non-generating buses are set to zero. The H_{agg} was varied in the entire grid by multiplying the S_i with a common factor. Note that the Nigerian transmission network does not comprise tie-line connections and power transfer [13] [24]. The grid frequency

is operated uniformly at 50 Hz across the entire network.

Here, we choose 11 buses for the investigation. The fault location bus 24, two buses at the same geodesic distance (unweighted), $r = 2$ from fault location with no inertia (i.e., buses 8 and 10) and three buses with inertia (i.e., buses 22, 55, and 57). We again choose two buses at the same geodesic distance (unweighted), $r = 7$ with no inertia (i.e., buses 7 and 30) and three buses with inertia (i.e., buses 3, 28, and 69). The reason is that we want to investigate the effect of momentary reserve both in the vicinity of the reserve (i.e., near to the fault location) and at far distances from the injection node. We also want to understand how momentary reserve tentatively contributes to damping of disturbances as they propagate along the network. A reference to the network buses numbers are in [23].

Keeping all system parameters, generations, losses and loads constant under undisturbed operations, a synchronous machine outage event (disturbance/contingency) is induced at bus 24 at exactly $t = 5$s of the 90s transient electromechanical stability simulation time frame with a 200ms switching, enabling the observations on the buses in PowerFactory power simulation software. The change in frequency propagated across the grid is related to the change of power in (10). The Figure 3 shows the frequency dynamics at a network bus. Here, the red line marks the frequency magnitude at final settling time. The black arrows point to the local maxima or minima of the frequency magnitude and arrival times. From this nodal points described in Figure 3, we observe at each study case node, the frequency's time of arrival (ToA), defined as the time the frequency deviation first reaches a small threshhold of $\delta\nu = \pm 0.002$ Hz, as defined in more detail in [23]. Furthermore we record the time of the first maximum (maxima_t) of the transient and its magnitude ($\text{maxima}_{\text{mag}}$), the time of the first minimum (minima_t) and its magnitude ($\text{minima}_{\text{mag}}$). We also observe the final frequency's settling time (FS_t), its magnitude (FS_{mag}) and frequency deviation (Dev_{mag}) from the nominal 50Hz value, for each of these nodes. For case studies I-V in Tables I-V, we show the observations in milliseconds for the case study nodes, with static network power flow of the Nigerian transmission grid.

TABLE I: N-NODAL OBSERVATIONS WITH LARGE DISTURBANCE AND NO RESERVE AT FAULT LOCATION GIVEN THAT $H_{\text{agg}} = 2$s

Bus	r	ToA (s)	minima_t (s)	$\text{minima}_{\text{mag}}$ (Hz)	FS_t (s)	FS_{mag} (Hz)	Dev_{mag} (Hz)
24	0	5.012	6.522	49.596	27.200	49.829	0.171
8	2	5.012	6.522	49.596	27.201	49.829	0.171
10	2	5.012	6.522	49.596	27.200	49.829	0.171
22	2	5.013	6.282	49.596	27.195	49.829	0.171
55	2	5.013	6.532	49.596	27.201	49.829	0.171
57	2	5.012	6.532	49.597	27.196	49.829	0.171
7	7	5.013	6.372	49.598	27.205	49.829	0.171
30	7	5.013	6.322	49.600	27.206	49.829	0.171
3	7	5.013	6.422	49.590	27.185	49.829	0.171
28	7	5.013	6.942	49.596	27.184	49.829	0.171
69	7	5.013	6.352	49.592	27.186	49.829	0.171

TABLE II: N-NODAL OBSERVATIONS WITH LARGE DISTURBANCE AND LARGE RESERVE AT FAULT LOCATION GIVEN THAT $H_{\text{agg}} = 2$s

Bus	r	ToA (s)	minima_t (s)	$\text{minima}_{\text{mag}}$ (Hz)	FS_t (s)	FS_{mag} (Hz)	Dev_{mag} (Hz)
24	0	5.014	6.132	49.920	25.700	49.967	0.033
8	2	5.014	6.112	49.920	25.691	49.967	0.033
10	2	5.014	6.102	49.920	25.690	49.967	0.033
22	2	5.015	6.282	49.919	25.687	49.967	0.033
55	2	5.014	6.082	49.920	25.691	49.967	0.033
57	2	5.015	6.192	49.919	25.688	49.967	0.033
7	7	5.016	6.292	49.920	25.696	49.967	0.033
30	7	5.016	6.372	49.920	25.698	49.967	0.033
3	7	5.017	6.252	49.918	25.679	49.967	0.033
28	7	5.017	6.142	49.916	25.678	49.967	0.033
69	7	5.017	6.182	49.918	25.680	49.967	0.033

TABLE III: N-NODAL OBSERVATIONS WITH LARGE DISTURBANCE AND LARGE RESERVE AT FAULT LOCATION GIVEN THAT $H_{\text{agg}} = 6$s

Bus	r	ToA (s)	minima_t (s)	$\text{minima}_{\text{mag}}$ (Hz)	FS_t (s)	FS_{mag} (Hz)	Dev_{mag} (Hz)
24	0	5.015	9.312	49.928	29.304	49.967	0.033
8	2	5.015	9.262	49.928	29.304	49.967	0.033
10	2	5.015	9.272	49.928	29.304	49.967	0.033
22	2	5.017	8.352	49.928	29.302	49.967	0.033
55	2	5.015	9.442	49.928	29.305	49.967	0.033
57	2	5.017	9.142	49.928	29.302	49.967	0.033
7	7	5.019	9.182	49.928	29.308	49.967	0.033
30	7	5.020	8.932	49.928	29.309	49.967	0.033
3	7	5.028	8.672	49.927	29.296	49.967	0.033
28	7	5.074	8.602	49.927	29.295	49.967	0.033
69	7	5.029	8.652	49.927	29.296	49.967	0.033

TABLE IV: N-NODAL OBSERVATIONS WITH LARGE DISTURBANCE AND LARGE RESERVE AT FAULT LOCATION AND AN INCREASED RESERVE AT BUS 22 GIVEN THAT $H_{\text{agg}} = 2$s

Bus	r	ToA (s)	minima_t (s)	$\text{minima}_{\text{mag}}$ (Hz)	FS_t (s)	FS_{mag} (Hz)	Dev_{mag} (Hz)
24	0	5.014	6.612	49.920	27.645	49.967	0.033
8	2	5.014	6.122	49.921	27.647	49.967	0.033
10	2	5.014	6.612	49.920	27.645	49.967	0.033
22	2	5.015	6.352	49.919	27.641	49.967	0.033
55	2	5.014	6.582	49.920	27.647	49.967	0.033
57	2	5.015	6.152	49.921	27.642	49.967	0.033
7	7	5.016	6.342	49.921	27.653	49.967	0.033
30	7	5.016	6.452	49.921	27.655	49.967	0.033
3	7	5.017	6.282	49.919	27.630	49.967	0.033
28	7	5.017	6.142	49.917	27.629	49.967	0.033
69	7	5.017	6.252	49.919	27.631	49.967	0.033

TABLE V: N-NODAL OBSERVATIONS WITH LARGE DISTURBANCE AND LARGE RESERVE AT FAULT LOCATION AND WITH A NEWLY INSTALLED RESERVE AT BUS 7 GIVEN THAT $H_{\text{agg}} = 2$s

Bus	r	ToA (s)	minima_t (s)	$\text{minima}_{\text{mag}}$ (Hz)	FS_t (s)	FS_{mag} (Hz)	Dev_{mag} (Hz)
24	0	5.014	6.662	49.920	39.118	49.967	0.033
8	2	5.014	6.632	49.920	39.116	49.967	0.033
10	2	5.014	6.662	49.920	39.118	49.967	0.033
22	2	5.015	6.332	49.918	39.127	49.967	0.033
55	2	5.014	6.632	49.920	39.115	49.967	0.033
57	2	5.015	6.202	49.919	39.124	49.967	0.033
7	7	5.016	6.602	49.920	39.102	49.967	0.033
30	7	5.016	6.492	49.920	39.097	49.967	0.033
3	7	5.017	6.292	49.919	39.149	49.967	0.033
28	7	5.017	6.152	49.917	39.151	49.967	0.033
69	7	5.017	6.272	49.919	39.148	49.967	0.033

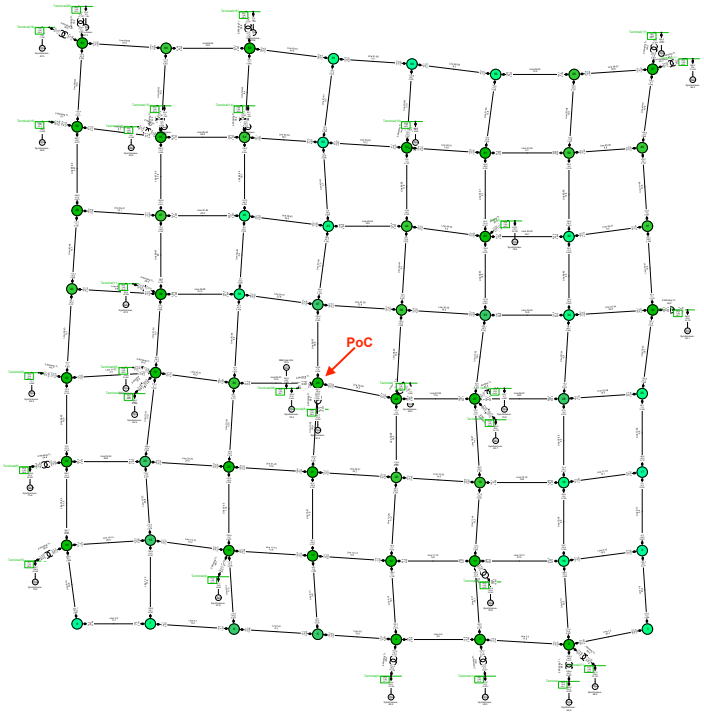

Figure 4: The Square 330 kV Power Grid. The Red pointer is the Point of Contingency (PoC, i.e., fault location) [23].

In Table I and with network H_{agg} at 2s, a typical behaviour of high renewable energy source injected grids, we observe a high frequency deviation (i.e., 0.171 Hz) induced by the large disturbance (of 1320MW power magnitude outage) at bus 24 fault location. We also observe that the disturbance arrived at the fault location first and at the same time as most of its nearest neighbours at $r = 2$, but arrived a little later at the distant buses 7, 30, 28 and 69. The frequency dip described by the minima$_{mag}$ shows the lowest magnitude of frequency deviation before the actions of turbines' governors.

At $H_{agg} = 2$s and in comparison with Table I, Table II shows the observations when the fault location is injected with inertia and large reserve. We observe that there are delays in the frequency ToA at the buses, a reduction in minima$_t$, which corresponds to increased frequency dips (i.e., minima$_{mag}$), shorter final frequency settling times with smaller magnitudes and hence, a decrease in the frequency deviation from the nominal value (0.033 Hz).

In Table III, we kept the network parameters constant and only increased the grid inertia, $H_{agg} = 6$s using (11) without changing the active power injections at any network node. We did not observe any further decrement in the frequency deviation or any increment in the frequency final settling magnitude, rather we observe a delay in its time of arrival at the buses with a corresponding increase in its dip and final settling time. This suggests that increasing the H_{agg} without a corresponding increase in the reserve does not improve the frequency dynamics during contingencies, rather it increases the arrival time of the disturbance while reducing the frequency dip across the network (i.e., improved minima$_{mag}$). This further delay in ToA also increases the frequency final settling time.

Table IV shows our nodal observations on the case study buses when we injected more power reserve prior to contingency at another bus with $r = 2$, from the fault location and keeping all other system operation parameters constant from observations in Table II. Here, the generator's power and reserve at the fault location are higher in magnitude than the injected ones. We observe that the frequency final settling magnitude did not increase, the ToA at the buses remained the same but there is an observable reduction in the frequency dip at some nodes.

To investigate the effect of the same reserve at a bus geometrically farther away from the fault location but with a higher degree of connectivity, which defines the number of edges connected to it, we removed the reserve at bus 22 with a node degree of 2 and installed it at another bus with $r = 7$ but with a node degree of 5 and keeping all other system operation parameters constant from our observations in Table II. The result of this new installation in Table V compared with Table IV shows no observable change in the frequency ToA at the buses and in the frequency final settling magnitude. Rather, we observe a delay in frequency dip time (i.e., minima$_t$) with a further delay in the final frequency settling time at the buses.

To further understand and verify if the above findings on the influence of momentary reserves would be general in different power network topological settings with special emphasis on

network's degree of meshedness, which is calculated by the coefficient of meshedness given as [25],

$$\phi_M = \frac{N_{\mathrm{E}} - N_B + 1}{2N_B - 5}, \tag{12}$$

where N_{E} and N_B are respectively the total number of transmission edges/lines and buses, we transformed the Nigerian 330 kV transmission network (N) into a Square power grid (i.e., S or S-grid) as shown in Figure 4. Note: ϕ_M has a maximum value of 1 for a completely meshed power grid. The ϕ_M for Nigerian 330 kV grid is 0.11 while that of Square power grid is calculated to be 0.40. See Ref: [23] for the details of the transformation.

In the Square grid shown in Figure 4, we choose for the purpose of verification, the point of contingency (i.e., bus 29), buses 13 and 20 with no inertia and bus 31 with inertia, all at the same geodesic distance of r= 2 from fault location. Also, at a geodesic distance of r= 5 from fault location, we choose buses 42 and 48 with no inertia and bus 55 with inertia. We choose r= 5 in the Square power grid because of the inertia criterion of selection and the limited number of buses with r= 7 from the fault location. Keeping all system parameters constant and inducing a synchronous machine event at bus 29 exactly at t =5s in a 90s transient electromechanical simulation time frame, we measure the change in frequency transmitted across the grid by this disturbance by placing a small threshold at $\delta\nu = \pm 0.002$ Hz exactly as in the case of the Nigerian transmission network studies. Again, we show the dynamic observations in milliseconds for the case study nodes, with static Square network power flow, recording the ToA, minima_t, maxima_t, (FS_t), $\mathrm{FS}_{\mathrm{mag}}$ and $\mathrm{Dev}_{\mathrm{mag}}$. For case studies in Tables VI-X similar to the ones studied in Tables I-V.

In Table VI and with H_{agg} at 2s in comparison with Table I, we again observe a high frequency deviation (i.e., 0.187 Hz) effected by the same large disturbance magnitude but induced at bus 29 point of contingency (PoC). Here, we observe the disturbance arrived at the PoC first but the arrival at the neighbouring buses with r= 2 are exponentially delayed. As geodesic distance, r is increasing from the PoC, the frequency dip described by the minima_t is reducing while the $\mathrm{minima}_{\mathrm{mag}}$ of the buses are increasing as expected.

At H_{agg} = 2s and in comparison with Table VI, Table VII shows the observations when the PoC is injected with inertia and a large reserve. We observe that the delays in the frequency ToA at the buses improved. There are reductions in the minima_t with correspondingly improved frequency dips (i.e., $\mathrm{minima}_{\mathrm{mag}}$) similar to Table II and with reductions in the final frequency settling time (FS_t) and magnitude ($\mathrm{FS}_{\mathrm{mag}}$). These lead to a decrease in the frequency deviation, $\mathrm{Dev}_{\mathrm{mag}}$ value (0.035 Hz) from the nominal.

In Table VIII, we increased only the grid inertia, H_{agg} = 6s by using (11) without changing the active power injections at any network bus and keeping all other network parameter constant as in Table VII. Again, we did not observe any change in the frequency deviation or any increment in the frequency final settling magnitude, rather we observe a delay in the frequency's ToA at the buses increasing with geodesic distance (r) and with a corresponding increase in the frequency dip (minima_t) and final settling times. This again suggests that increasing the H_{agg} alone without a corresponding increase in the reserve provides a delay in propagation of disturbances while reducing the frequency dip across the network (i.e., improved $\mathrm{minima}_{\mathrm{mag}}$). However, it does not improve the $\mathrm{Dev}_{\mathrm{mag}}$ during contingencies. This further delay in ToA resulting from increasing the H_{agg} also increases the frequency final settling times, similar to our observations in Table III above.

Table IX shows our nodal observations on the Square grid case study buses when we injected more power reserve prior to contingency at bus 31 with $r = 2$ from the PoC and keeping all other system operation parameters constant from the observations in Table VII. Here, the power capacity of the generator and reserve at the PoC are higher in magnitude than the injected one.

TABLE VI: S-NODAL OBSERVATIONS WITH LARGE DISTURBANCE AND NO RESERVE AT FAULT LOCATION GIVEN THAT $H_{\mathrm{agg}} = 2$s

Bus	r	ToA (s)	minima_t (s)	$\mathrm{minima}_{\mathrm{mag}}$ (Hz)	FS_t (s)	$\mathrm{FS}_{\mathrm{mag}}$ (Hz)	$\mathrm{Dev}_{\mathrm{mag}}$ (Hz)
29	0	5.001	6.243	49.562	27.500	49.813	0.187
13	2	5.002	6.302	49.566	27.496	49.813	0.187
20	2	5.002	6.372	49.564	27.496	49.813	0.187
31	2	5.003	6.202	49.565	27.500	49.813	0.187
42	5	5.003	6.512	49.562	27.503	49.813	0.187
48	5	5.004	6.142	49.569	27.506	49.813	0.187
55	5	5.005	6.132	49.569	27.505	49.813	0.187

TABLE VII: S-NODAL OBSERVATIONS WITH LARGE DISTURBANCE AND LARGE RESERVE AT FAULT LOCATION GIVEN THAT $H_{\mathrm{agg}} = 2$s

Bus	r	ToA (s)	minima_t (s)	$\mathrm{minima}_{\mathrm{mag}}$ (Hz)	FS_t (s)	$\mathrm{FS}_{\mathrm{mag}}$ (Hz)	$\mathrm{Dev}_{\mathrm{mag}}$ (Hz)
29	0	5.007	6.072	49.915	27.275	49.965	0.035
13	2	5.015	6.242	49.916	27.273	49.965	0.035
20	2	5.013	6.452	49.916	27.274	49.965	0.035
31	2	5.020	6.202	49.915	27.278	49.965	0.035
42	5	5.023	6.532	49.916	27.282	49.965	0.035
48	5	5.027	6.142	49.917	27.285	49.965	0.035
55	5	5.030	6.142	49.917	27.284	49.965	0.035

TABLE VIII: S-NODAL OBSERVATIONS WITH LARGE DISTURBANCE AND LARGE RESERVE AT FAULT LOCATION GIVEN THAT $H_{\mathrm{agg}} = 6$s

Bus	r	ToA (s)	minima_t (s)	$\mathrm{minima}_{\mathrm{mag}}$ (Hz)	FS_t (s)	$\mathrm{FS}_{\mathrm{mag}}$ (Hz)	$\mathrm{Dev}_{\mathrm{mag}}$ (Hz)
29	0	5.010	9.272	49.925	30.357	49.965	0.035
13	2	5.020	8.732	49.925	30.356	49.965	0.035
20	2	5.019	8.682	49.925	30.356	49.965	0.035
31	2	5.028	9.032	49.925	30.359	49.965	0.035
42	5	5.031	8.652	49.925	30.361	49.965	0.035
48	5	5.042	9.312	49.925	30.363	49.965	0.035
55	5	5.055	9.412	49.925	30.363	49.965	0.035

TABLE IX: S-NODAL OBSERVATIONS WITH LARGE DISTURBANCE AND LARGE RESERVE AT FAULT LOCATION AND AN INCREASED RESERVE AT BUS 31 GIVEN THAT $H_{agg} = 2$s

Bus	r	ToA (s)	minima$_t$ (s)	minima$_{mag}$ (Hz)	FS$_t$ (s)	FS$_{mag}$ (Hz)	Dev$_{mag}$ (Hz)
29	0	5.007	6.452	49.917	27.618	49.966	0.034
13	2	5.015	6.382	49.919	27.615	49.966	0.034
20	2	5.014	6.422	49.918	27.616	49.966	0.034
31	2	5.023	6.212	49.915	27.700	49.966	0.034
42	5	5.023	6.582	49.917	27.625	49.966	0.034
48	5	5.028	6.182	49.918	27.630	49.966	0.034
55	5	5.031	6.082	49.919	27.628	49.966	0.034

TABLE X: S-NODAL OBSERVATIONS WITH LARGE DISTURBANCE AND LARGE RESERVE AT FAULT LOCATION AND AN INCREASED RESERVE AT BUS 55 GIVEN THAT $H_{agg} = 2$s

Bus	r	ToA (s)	minima$_t$ (s)	minima$_{mag}$ (Hz)	FS$_t$ (s)	FS$_{mag}$ (Hz)	Dev$_{mag}$ (Hz)
29	0	5.007	6.462	49.917	27.562	49.966	0.034
13	2	5.015	6.412	49.919	27.561	49.966	0.034
20	2	5.014	6.442	49.918	27.562	49.966	0.034
31	2	5.021	6.222	49.915	27.566	49.966	0.034
42	5	5.023	6.532	49.917	27.570	49.966	0.034
48	5	5.028	6.162	49.918	27.574	49.966	0.034
55	5	5.032	6.142	49.918	27.572	49.966	0.034

We observe that the final frequency settling magnitude increased by 1 mHz, the ToAs at the buses relatively increased but there is an observable delay in the minima$_t$ with improvements in the magnitude of the frequency dips as the geodesic distance increases.

Furthermore, to investigate the effect of the same reserve at a bus geometrically farther with r= 5 from the PoC but with the same degree of connectivity, we keep all other system operation parameters constant from our observations in Table VII. The result of this new reserve placement in Table X compared with Table IX shows little observable changes only in the frequency ToAs at buses 31 and 55, which happens to be the locations of inertia. We also observe no change in the final frequency settling magnitude. Also, we observe that the final frequency settling time at the buses improved but with no observable change in its magnitude (i.e., FS$_{mag}$) similar to our observations in the case study 5 in Table V.

From the above numerical experiments, we can note that the frequency ToA at any network bus is a function of system parameters, in particular inertia while the frequency dip time (i.e., Minima$_t$) and its final settling magnitude are respectively functions of turbine's governor time constant and reserves. we can then estimate the deviation in frequency and the resultant frequency magnitude from the mechanics of momentary reserve dynamics if we consider important times of arrival at various points on any network bus after contingency. If a bus with inertia and momentary reserve undergoes contingency specifically of power outage event type and in a low H_{agg} (i.e., high renewable energy source penetration), we can estimate the final frequency settling time (FS$_t$) at the network buses to be,

$$\mathrm{FS}_t = (T_{\mathrm{oA}} M_t) - T_{\mathrm{oA}} + \phi_M, \qquad (13)$$

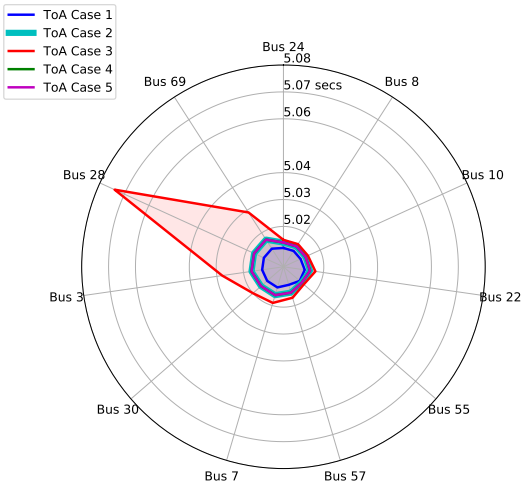

Figure 5: Visualization of Times of Arrival (ToA) in the Nigerian grid study cases I-V as tabulated in Tables I-V.

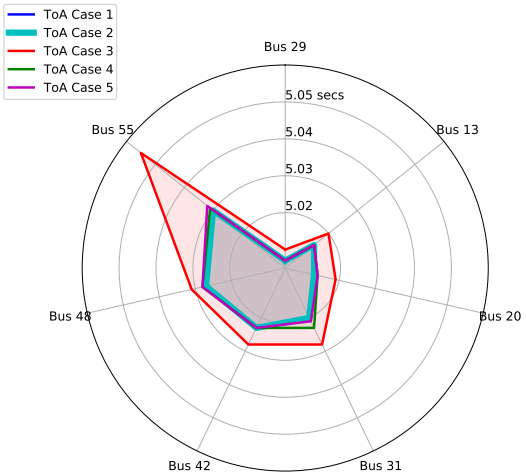

Figure 6: Visualization of Times of Arrival (ToA) in the Square grid study cases VI-X as tabulated in Tables VI-X.

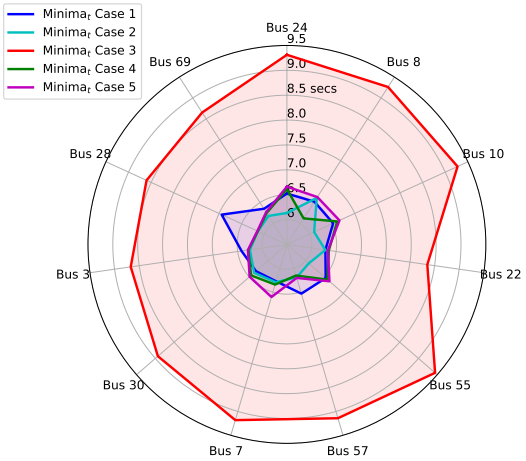

Figure 7: Visualization of frequency dip time (Minima$_t$) in the Nigerian grid study cases I-V as tabulated in Tables I-V.

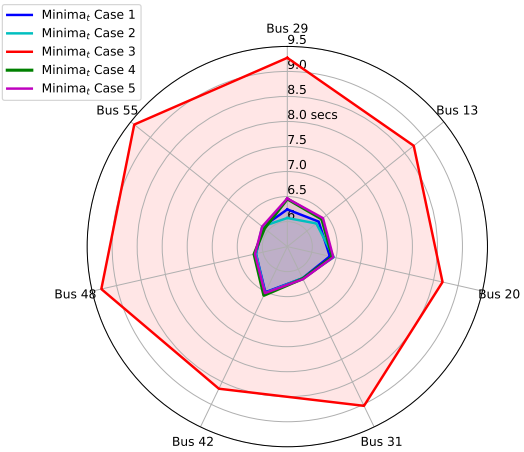

Figure 8: Visualization of frequency dip time (Minima$_t$) in Square grid study cases VI-X as tabulated in Tables VI-X.

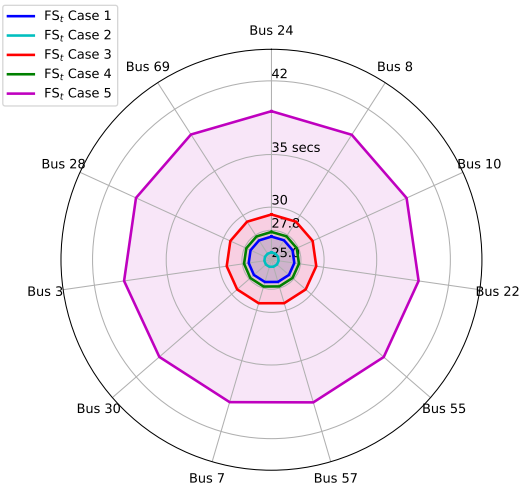

Figure 9: Visualization of final frequency settling time (FS$_t$) in the Nigerian grid study cases I-V as tabulated in Tables I-V.

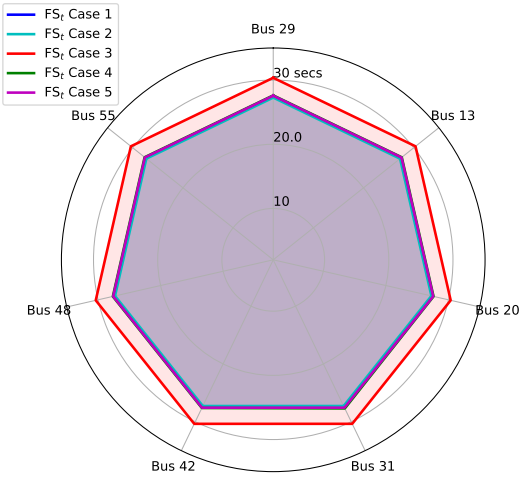

Figure 10: Visualization of final frequency settling time (FS$_t$) in the Square grid study cases VI-X as tabulated in Tables VI-X.

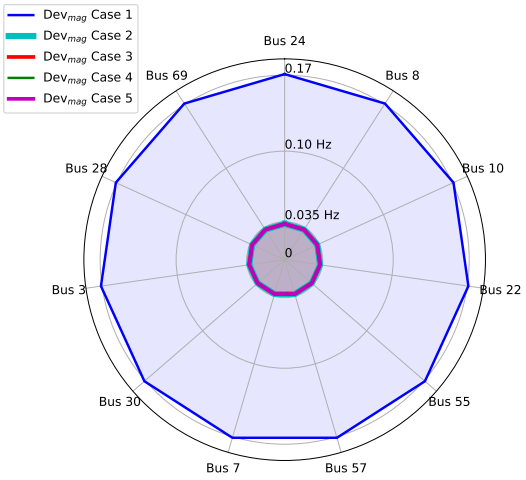

Figure 11: Visualization of final frequency deviation magnitude (Dev$_{\text{mag}}$) in the Nigerian grid study cases I-V as tabulated in Tables I-V.

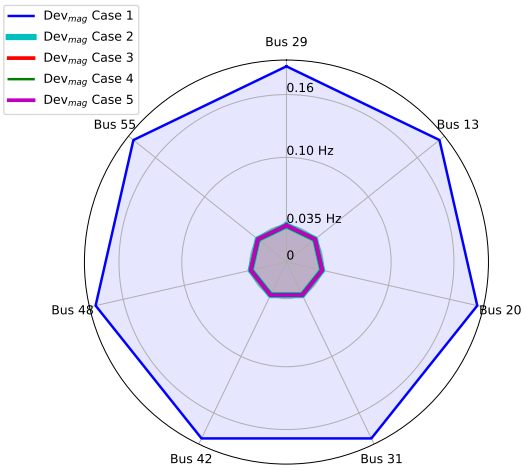

Figure 12: Visualization of final frequency deviation magnitude (Dev$_{\text{mag}}$) in the Square grid study cases VI-X as tabulated in Tables VI-X

where T_{oA} is the frequency time of arrival (ToA), ϕ_M is the grid's coefficient of meshedness as defined in Section IV and M_t is an abbreviation of Minima$_t$, which is a function of speed-droop characteristics of turbine governor defined in (10). The value of FS$_t$ in (13) is true provided that H_{agg} is low. With more momentary reserve distribution at contingent neighbouring buses in the low inertia grid, FS$_t$ can be estimated and given as,

$$\text{FS}_t = (T_{\text{oA}} M_t) + T_{\text{oA}} + \phi_M. \tag{14}$$

However, if a network has a high H_{agg} (e.g. $H_{\text{agg}} = 6$s) with no corresponding increment in the magnitude of momentary reserves, we can estimate FS$_t$ at the network buses to be,

$$\text{FS}_t = (T_{\text{oA}} M_t) - T_{\text{oA}} - M_t - \phi_M. \tag{15}$$

Irrespective of the conditions for the value of FS$_t$ in (13) - (15), the resultant final frequency settling magnitude (with unit in

Hertz) as a result of $1/\mathrm{FS}_t$ deviation can now be estimated as,

$$\mathrm{FS}_{\mathrm{mag}} = \nu_1 - \frac{1}{\mathrm{FS}_t}, \tag{16}$$

where ν_1 and $\mathrm{FS}_{\mathrm{mag}}$ are the pre-contingent and post-contingent network bus frequencies, respectively. The value of ν_1 at normal operation is ν_0 (i.e., 50 or 60 Hz).

V. Results Summary

To properly summarize the characteristics of the case study grids, we combine the 5 study cases in spider graphs to enhance the visualizations, differences and similarities between these grids with different topologies and degree of meshedness (ϕ_M). We reiterate that an increase in the nodal momentary reserve generally delays the travel and arrival of disturbances in a power grid at contingencies as shown in Figures 5 and 7. These observations are found to be similar to the ones in Figures 6 and 8, respectively. In particular, momentary reserves improve the frequency magnitudes at the local minima points and reduces the final frequency settling time in Nigerian network as shown in Figures 7 and 9. These findings are also valid for the Square grid as respectively shown in Figures 8 and 10 but in addition, we observe that its final frequency arrival times are more clustered. This is maybe due to its high degree of meshedness.

Moreover, we found out that the optimal placement of momentary reserve is at the point of contingency as it contributes more in the damping of disturbance across the network more than at any other place as visualized in Figures 11 and 12. Since we may not always be able to predict a fault location, the optimal solution would be to place momentary reserve at all buses where resources and costs allow. In this way, the power system could quickly recover most contingencies within few seconds after their occurrences. Again, we observed that injecting momentary reserve at a bus with high connectivity does not improve the frequency dip time (i.e., minima_t) and final settling time at the buses if the bus is geometrically farther away from the fault location. Hence, the farther away the reserve is from the fault location, the more time it would take for the frequency to stabilize at the buses.

Also, we conclude that increasing the grid inertia without a corresponding increase in the magnitude of the reserve could only delay the travel and arrival of disturbances in electrical network but does not reduce the frequency deviation from the nominal value as seen in case study 3, irrespective of the grid's ϕ_M. Moreover, we established an estimation for the final frequency settling time and magnitude at network buses after contingency, especially of power outage event type. These results would be important to the Transmission System Operators (TSOs) when injecting virtual inertia in the energy transition to renewable schemes.

VI. conclusion

In this paper, we have studied the dynamics of power system reserves in a realistic model of Nigerian power grid as well as synthetic Square power network. By realistic numerical experiments, we explored the mechanisms of momentary reserve contributions to the damping of system oscillations at contingencies and thereby work to restore the grid frequency to its nominal value. We have shown that the optimal placement of momentary reserve in a highly penetrated renewable energy source grid would be at the fault location (i.e., PoC), particularly in the case of generator outage events at plant stations irrespective of the network's degree of meshedness. Since this situation could not always be predicted, we suggest placement of reserves at all nodes where resources permit as this would improve the overall final frequency settling time, frequency dip, and reduce overall frequency deviation from the nominal value, thereby contributing to primary frequency control and reducing the amount of secondary control power needed.

Acknowledgment

We gratefully acknowledge the support of Bundesministerium für Bildung und Forschung (BMBF) CoNDyNet-2, FK. 03EK3055D.

References

[1] K.P. Nnoli and S. Kettemann, "Dynamics of momentary reserves under contingency: Observations from numerical experiments," *ENERGY 2021, The Eleventh International Conference on Smart Grids, Green Communications and IT Energy-Aware Technologies*, 2021.

[2] K. Shi, H. Ye, W. Song, and G. Zhou, "Virtual inertia control strategy in microgrid based on virtual synchronous generator technology," *IEEE Access*, vol. 6, pp. 27 949–27 957, 2018.

[3] P. Kundur, *Power System Stability and Control*. McGraw-Hill, New York, 1994.

[4] J. Machowski, J. Bialek, and J. R. Bumby, *Power System Dynamics: Stability and Control*. Wiley, 2008.

[5] P. Anderson and A. Fouad, "Power system control and stability," *Iowa State University Press, Ames, Iowa*, vol. 1, 1977.

[6] DigSILENT GmbH, *PowerFactory version 2020 Software Manual*, Heinrich-Hertz-Straße 9, 72810, Gomaringen, Germany, 2020.

[7] M. Rajagopalan and M. Rautkivi, "System level value of power system reserve optimization in Singapore and South Korea." Power-Gen Asia, 2014.

[8] Y. Zhang, J. Tan, I. Krad, R. Yang, V. Gevorgian, and E. Ela, *Investigating power system primary and secondary reserve interaction under high wind power penetration*. National Renewable Energy Laboratory (NREL), 2016.

[9] UCTE, "Load-frequency control and performance," *UCTE Operation Handbook Policy 1*, 2004.

[10] P. Kundur, J. Paserba, V. Ajjarapu, G. Andersson, A. Bose, C. Canizares, N. Hatziargyriou, D. Hill, A. Stankovic, C. Taylor, T. V. Cutsem, and V. Vittal, "Definition and classification of power system stability," *IEEE Transactions on Power Systems*, vol. Vol. 19, No. 2, (2004).

[11] A. A. Sallam and O. P. Malik, *Power system stability: Modelling, analysis and control*. IET Power and Energy Series 76, 2015.

[12] G. Tan, C. Xu, F. Wu, C. Qi, D. Wang, P. Yang, and Y. Feng, "Research on primary frequency regulation of wind turbine based on new nonlinear droop control," in *2020 4th International Conference on HVDC (HVDC)*, 2020, pp. 170–174.

[13] K. P. Nnoli, "Implementation of a dynamic network model of the Nigerian transmission grid for investigations on power system stability," *https://doi.org/10.31224/osf.io/r82zn*, 2019.

[14] National Control Center Osogbo, "Transmission data update of the transmission company of Nigeria," *Field Research at National Transmission Company of Nigeria in March*, 2019.

[15] ENTSO-E, *Documentation on controller test in test grid configurations*. Entso-E, 2013.

[16] G. Rogers, "Demystifying power system oscillations," *IEEE Computer Applications in Power*, vol. 9, no. 3, pp. 30–35, 1996.

[17] IEEE Power Engineering Society, *IEEE guide for synchronous generator modelling practice and applications in power system stability analysis*. IEEE Press, 2002.

[18] IEEE Power and Energy Society, *Dynamic models for turbine-governor in power system studies*. IEEE Press, 2013.

[19] A. R. Bergen and D. J. Hill, "A structure preserving model for power system stability analysis," *IEEE Transactions on Power Apparatus and Systems*, vol. PAS-100, no. 1, pp. 25–35, 1981.

[20] D. Manik, M. Rohden, H. Ronellenfitsch, X. Zhang, S. Hallerberg, D. Witthaut, and M. Timme, "Network susceptibilities: Theory and applications," *Physical Review E 95, 012319*, 2017.

[21] K.P. Nnoli, S. Kettemann, "Supplementary material in DataPort," *[IEEE DataPort] https://dx.doi.org/10.21227/pjpt-nk47*, 2021.

[22] A. Ulbig, T. S. Borsche, and G. Anderson, "Impact of low rotational inertia on power system stability and control," vol. 14, no. 3, pp. 7290–7297, 2014.

[23] K.P. Nnoli and S. Kettemann, "Spreading of disturbances in realistic models of transmission grids: Dependence on topology, inertia and heterogeneity," *[engrarxiv] https://dx.doi.org/10.31224/osf.io/c8awt*, 2021.

[24] Nigerian Electricity Regulatory Commission (NERC), *The grid code for the Nigerian electricity transmission system*. NERC Press, 2014.

[25] J. Buhl, J. Gautrais, N. Reeves, R. V. Solé, S. Valverde, P. Kuntz, and G. Theraulaz, "Topological patterns in street networks of self-organized urban settlements," *The European Physical Journal B*, vol. 49, no. 4, pp. 513–522, 2006.